Supplement of Atmos. Chem. Phys., 26, 1001–1020, 2026
https://doi.org/10.5194/acp-26-1001-2026-supplement

Atmospheric Chemistry and Physics
Open Access
EGU

Supplement of

Evaluating simulations of organic aerosol volatility and degree of oxygenation in eastern China

Yu Li et al.

Correspondence to: Momei Qin (momei.qin@nuist.edu.cn)

This PDF file includes:

Supplementary Notes S1-S2

Supplementary Tables S1-S10

Supplementary Figures S1-S21

Supplementary References

S1. Estimation of L/S/IVOC Emissions

The L/S/IVOC emission inventory was developed based on VOC and POA emissions from MEICv1.4, considering the strong correlation between IVOC and VOC emissions and similar definitions of POA and S/LVOCs. In MEICv1.4, emissions are classified into five major source categories (power plants, industry, residential, transportation, and agriculture) and further divided into 22 subcategories. IVOC emissions for each subcategory were estimated using source-specific scaling factors ($f_{IVOC,i,j}$) applied to total VOC emissions, as expressed in Equation S1. S/LVOC emissions resulted from the semi-volatile fraction of POA were estimated using the corresponding scaling factor ($f_{S/LVOC,i,j}$) relative to POA, as shown in Equation S2. IVOC and S/LVOC emissions were then distributed into four volatility bins: 10^3 μg m^{-3} to 10^6 μg m^{-3} for IVOCs and 10^{-2} μg m^{-3} to 10^2 μg m^{-3} for S/LVOCs, with an interval of one order of magnitude per bin. The equations are as follows:

$$E_{IVOC,i,j} = E_{VOC,i,j} * f_{IVOC,i,j} \quad \text{(S1)}$$

$$E_{SLVOC,i,j} = E_{POA,i,j} * f_{S/LVOC,i,j} \quad \text{(S2)}$$

Here, i represents the emission source category, j denotes the volatility bin, and $E_{IVOC,i,j}$ and $E_{SLVOC,i,j}$ are the estimated IVOC and S/LVOC emissions (in tons) for each source i and bin j. The scaling factors f were obtained from the literature, with more details provided in Table S3.

S2. Calculation of glass transition temperature (T_g) and viscosity

The glass transition temperature of OA under dry conditions ($T_{g,org}$) is calculated by the Gordon-Taylor equation (Gordon and Taylor, 1952) by assuming the Gordon-Taylor constant (k_{GT}) of 1 (Dette et al., 2014):

$$T_{g,org} = \sum_i \omega_i T_{g,i} \quad \text{(S3)}$$

where ω_i represents the mass fraction of each OA species in CMAQ.

The glass transition temperature of the organic-water mixture ($T_{g,\omega org}$) is determined using the Gordon-Taylor equation, as expressed in Equation (S4):

$$T_{g,\omega org} = \frac{(1-\omega_{org})T_{g,w} + \frac{1}{k_{GT}}\omega_{org}T_{g,org}}{(1-\omega_{org}) + \frac{1}{k_{GT}}\omega_{org}} \quad \text{(S4)}$$

where k_{GT} = 2.5 is assumed, and $T_{g,w}$ (the glass transition temperature of water) is set to 136 K (Kohl et al., 2005). The mass fraction of OA in the particulate phase (ω_{org}) is given by Equation S5:

$$\omega_{org} = \frac{m_{OA}}{m_{OA} + m_{H_2O}} \quad \text{(S5)}$$

The mass concentration of water (m_{H_2O}) can be determined from the effective hygroscopicity parameter (κ) of OA:

$$m_{H_2O} = \left(\frac{a_w}{1-a_w}\right)\frac{\kappa\rho_w m_{OA}}{\rho_{OA}} \quad \text{(S6)}$$

$$\kappa_{org,i} = 0.11\frac{OM}{OC} - 0.10 \quad \text{(S7)}$$

Here, the κ_{org} of each species was parameterized as a function of OM/OC (Pye et al., 2017). ρ_w (water density) and ρ_{OA} (OA density) are assumed to be 1 and 1.44 g cm^{-3}, respectively, based on observational experiments in DY. The water activity (a_w) is derived from the relative humidity (RH) as $a_w = RH/100$.

Supplementary Tables

Table S1 Statistical metrics of meteorological parameters in DY and GZ.

Parameter	Metrics	DY	GZ	Benchmark
T2 (℃)	OBS	12.99	24.34	
	SIM	13.00	24.32	
	MB	0.01	0.01	≤±0.5
	ME	2.00	1.79	≤2
	RMSE	2.55	2.39	
RH (%)	OBS	49.14	68.07	
	SIM	46.91	64.20	
	MB	-2.23	-3.87	
	ME	9.79	8.66	
	RMSE	12.87	11.22	
WS (m/s)	OBS	3.82	2.45	
	SIM	5.17	3.19	
	MB	**1.34**	**0.74**	≤±0.5
	ME	1.98	1.27	≤2
	RMSE	2.45	1.59	≤2
WD (°)	OBS	159.33	94.64	
	SIM	151.39	66.41	
	MB	**155.51**	**63.97**	≤±10
	ME	**155.52**	**64.03**	≤±30
	RMSE	181.78	107.52	

[a] $MB = \frac{1}{N}\sum_{i=1}^{N}(M_i - O_i)$; $ME = \frac{1}{N}\sum_{i=1}^{N}|M_i - O_i|$; $RMSE = \left[\frac{1}{N}\sum_{i=1}^{N}(M_i - O_i)^2\right]^{\frac{1}{2}}$, where M_i and O_i represent model predictions and observations, respectively, and N is the number of data. The benchmarks refer to Emery and Tai (2001).

Table S2 Statistical metrics of predicted O_3, NO_2, SO_2 and $PM_{2.5}$ in DY and GZ.

Site	Pollutant	Case	NMB	NME	r
DY	MDA8 O_3	1D-VBS	-0.09	0.18	0.82
		1D-VBS_E	-0.09	0.18	0.82
		1D-VBS_EY	-0.08	0.18	0.82
		2D-VBS	-0.09	0.18	0.82
	NO_2	1D-VBS	-0.26	0.49	0.53
		1D-VBS_E	-0.27	0.50	0.53
		1D-VBS_EY	-0.27	0.49	0.53
		2D-VBS	-0.27	0.49	0.53
	SO_2	1D-VBS	-0.41	0.51	0.47
		1D-VBS_E	-0.41	0.51	0.47
		1D-VBS_EY	-0.41	0.51	0.47
		2D-VBS	-0.41	0.51	0.47
	$PM_{2.5}$	1D-VBS	-0.58	0.58	0.82
		1D-VBS_E	-0.50	0.50	0.84
		1D-VBS_EY	-0.46	0.46	0.84
		2D-VBS	-0.46	0.46	0.83
GZ	MDA8 O_3	1D-VBS	0.26	0.49	0.38
		1D-VBS_E	0.25	0.49	0.38
		1D-VBS_EY	0.25	0.48	0.38
		2D-VBS	0.26	0.49	0.38
	NO_2	1D-VBS	-0.42	0.53	0.33
		1D-VBS_E	-0.42	0.53	0.33
		1D-VBS_EY	-0.42	0.53	0.33
		2D-VBS	-0.42	0.53	0.33
	SO_2	1D-VBS	-0.46	0.78	0.48
		1D-VBS_E	-0.46	0.78	0.48
		1D-VBS_EY	-0.46	0.78	0.48

	2D-VBS	-0.46	0.78	0.48
$PM_{2.5}$	1D-VBS	-0.48	0.50	0.33
	1D-VBS_E	-0.35	0.40	0.37
	1D-VBS_EY	-0.19	0.32	0.37
	2D-VBS	-0.31	0.38	0.45

[a]Benchmark values are NMB<±0.15, NME<0.25, and R>0.5 for MDA8 O_3, NMB<±0.3, NME<0.5, and R>0.4 for 24-hr average $PM_{2.5}$, $NMB = \frac{\sum_{i=1}^{N}(M_i - O_i)}{\sum_{i=1}^{N} O_i}$; $NME = \frac{\sum_{i=1}^{N}|M_i - O_i|}{\sum_{i=1}^{N} O_i}$; $r = \frac{\sum_{i=1}^{N}[(M_i - \bar{M}) \times (O_i - \bar{O})]}{\sqrt{\sum_{i=1}^{N}(M_i - \bar{M})^2 \times \sum_{i=1}^{N}(O_i - \bar{O})^2}}$, where M_i and O_i represent model predictions and observations, $\bar{M}$ and $\bar{O}$ represent the mean of predictions and observations, and N is the number of data (Emery et al., 2017).

Table S3 Source-specific scaling factors for emissions of L/SVOCs ($\log_{10}C^*$(μg m^{-3})≤2) derived from POA emissions, and IVOCs (3≤$\log_{10}C^*$(μg m^{-3})≤6) derived from VOC emissions in this study.

Sector	Subsector	Fractions for logC*(μg m^{-3}, at 298K) bins									Ref.
		$f_{L/SVOC,i,j}$				$f_{IVOC,i,j}$					
		≤-2	-1	0	1	2	3	4	5	6	
Power	Power plants	0.2443	0.1304	0.0727	0.1454	0.4071	0.1880	0.1500	0.2260	0.1130	
Industry	industrial boiler	0.2443	0.1304	0.0727	0.1454	0.4071	0.1880	0.1500	0.2260	0.1130	Chang et al. (2022)
	heat supply										
	Cement										
	Coking	0.2355	0.1742	0.0805	0.0806	0.4291	0.0082	0.0075	0.0025	0.0017	
	Iron and steel										
	Petrochemicals										
	Oil and gas storage	0.0000	0.0000	0.0000	0.0000	0.0000	0.0000	0.0000	0.0000	0.12	[a]
	Industrial Painting					0.0025[c]	0.0127	0.0329	0.0405	0.1645	Mcdonald et al. (2018)
	architectural coating	0.0000	0.0000	0.0000	0.0000	0.0022[c]	0.0119	0.0290	0.0358	0.1455	
	printing					0.0021[c]	0.0103	0.0269	0.0331	0.1346	
	Other industrial sectors	0.5430	0.0958	0.0468	0.0614	0.2531	0.0385	0.0410	0.0563	0.1132	[b]

Residential	Domestic combustion	0.1072	0.2914	0.0377	0.0708	0.4928	0.0390	0.3170	0.2540	0.1200	Chang et al. (2022) [b]
	Domestic biomass combustion	0.4395	0.1923	0.0680	0.1387	0.1615	0.0690	0.1710	0.0480	0.0700	
	Domestic VCP	0.0000	0.0000	0.0000	0.0000	0.0030[c]	0.0156	0.0383	0.0469	0.1926	
	Other domestic sources	0.5156	0.1612	0.0352	0.0698	0.2181	0.0412	0.1754	0.1163	0.1275	
Transportation	Gasoline Vehicles	0.9869	0.0000	0.0031	0.0051	0.0045	0.0061	0.0206	0.0568	0.0943	Tang et al. (2021) [d]
	Diesel Vehicles	0.1321	0.0546	0.0858	0.3641	0.3633	0.0540	0.1490	0.1870	0.1590	
	Motorcycles	0.9869	0.0000	0.0031	0.0051	0.0045	0.0061	0.0206	0.0568	0.0943	Tang et al. (2021) [f]
	Non-Road transportation	0.7801	0.0307	0.0399	0.0645	0.0849	0.0147	0.0344	0.0684	0.0787	
Agriculture	Fertilizer Application Livestock Farming	0.0000	0.0000	0.0000	0.0000	0.0000	0.0000	0.0000	0.0000	0.0000	Chang et al. (2022) [b]

[a] Data from the California Air Resources Board's 2015 Consumer and Commercial Products Survey (CARB, 2019);

[b] Average values of subsectors under the same sector;

[c] Since volatile chemical product emissions are closely correlated with VOC emissions, the SVOC emissions for this sector were estimated based on VOC emissions.

[d] The IVOC scaling factors for diesel vehicles were referenced from Lu et al. (2020) , while the SVOC scaling factors were based on the work of An et al. (2023).

[f] For non-road mobile sources, scaling factors for agricultural machinery (Che et al., 2023) , road construction machinery (Shen et al., 2023), and ships (An et al., 2023), were used. The contributions of different sources to non-road mobile sources were obtained from Huang et al. (2018) and Zhao et al. (2022).

Table S4 Annual emissions of IVOCs and SVOCs (Unit: Tg) from different emission sources in China in 2018.

Sector	IVOCs	SVOCs
Industry and Power	1.17	0.34
Residential	1.91	2.69
Transportation	0.90	0.15
Solvent use	2.69	/
Total	6.68	3.18

Table S5 Mole-based SOA yields for aromatics and PAHs used in this study.

Case	Precursor	High NOx						Ref
		10E-06	**0.01**	**0.1**	**1**	**10**	**100**	
1D-VBS	Benzene	0.0000	0.0000	0.0000	0.0340	0.0000	0.3920	Qin et al. (2021)
	Toluene	0.0000	0.0000	0.0000	0.0160	0.0510	0.0470	
	Xylene	0.0000	0.0000	0.0000	0.0150	0.0230	0.0600	
	PAHs	0.0000	0.0000	0.0000	0.0280	0.0225	0.0280	
	Precursor	**Low NOx**						**Ref**
		10E-06	**0.01**	**0.1**	**1**	**10**	**100**	
	Benzene	0.0000	0.1460	0.0000	0.0000	0.0000	0.0000	Qin et al. (2021)
	Toluene	0.0000	0.1400	0.0000	0.0000	0.0000	0.0000	
	Xylene	0.0000	0.1930	0.0000	0.0000	0.0000	0.0000	
	PAHs	0.0000	0.0473	0.0000	0.0000	0.0000	0.0000	
Case	**Precursor**	**High NOx**						**Ref**
		10E-06	**0.01**	**0.1**	**1**	**10**	**100**	
1D-VBS_EY	Benzene	0.0000	0.0000	0.1874	0.1559	0.0000	0.0000	Bilsback et al. (2023)
	Toluene	0.0000	0.0000	0.1358	0.0967	0.0000	0.0000	
	Xylene	0.0000	0.0000	0.0284	0.0049	0.0040	0.1581	
	PAHs[a]	0.0000	0.1183	0.0988	0.1269	0.2110	0.0000	
	Precursor	**Low NOx**						**Ref**
		10E-06	**0.01**	**0.1**	**1**	**10**	**100**	
	Benzene	0.0017	0.0131	0.0000	0.0592	0.1732	0.0000	Bilsback et al. (2023)
	Toluene	0.0007	0.0299	0.0000	0.0703	0.1584	0.0000	
	Xylene	0.0106	0.0000	0.1452	0.0000	0.0422	1.3439	
	PAHs[a]	0.0230	0.0600	0.0381	0.0572	0.1753	0.0000	

[a] The parameters for PAHs adopted naphthalene SOA yields from Bilsback et al. (2023).

Table S6 Summary of O/C ratios for POA factors in eastern China reported in prior measurements.

Site	HOA	BBOA	CCOA	COA	NOA	Ref
Dongying	0.55	0.37	/	/	/	Feng et al. (2023)
Guangzhou	0.2	/	/	0.19	0.5	Chen et al. (2021)
Gucheng	0.13	0.44	0.15	/	/	Zhang et al. (2022)
Beijing	0.16	0.29	0.19	0.16	/	Xu et al. (2021)
Nanjing	0.12	/	/	0.27	/	Xian et al. (2023)
Nanjing	0.17	0.49	/	/	/	Gu et al. (2022)
Shanghai	0.15	/	/	0.29	/	Zhu et al. (2021)
Hangzhou	0.07	/	/	0.18/	/	Li et al. (2018)
Yangzhou	0.25	0.45	/	0.36	/	(Ge et al., 2017)
Average	0.2	0.41	0.17	0.24	0.5	

Table S7 OA surrogate species in the 1D-VBS and their physicochemical properties at 298K, including saturated vapor pressure (C_0^*), organic matter to organic carbon ratio (OM/OC), molecular weight ($\tilde{M}$), and oxygen to carbon ratio (O/C).

Species	Description	C_0^*	OM/OC	$\tilde{M}$	O/C	Ref
AAVB1	ASOA	0.01	2.7	198.0	1.227	Qin et al. (2021)
AAVB2		1	2.35	179.0	0.947	
AAVB3		10	2.17	169.0	0.803	
AAVB4		100	1.99	158.0	0.659	
AAVB5 [a]		0.1	2.53	189.0	1.091	Newly added
AAVB6 [a]		1E-06	3.41	229.0	1.797	
AOLGA	Oligomers derived from ASOA	1E-10	2.50	206.0	1.067	Pye et al. (2017)
AIETET	2-methyltetrols (2-MT)	1E-10	2.27	136.15	0.833	Pye et al. (2013)
AIEOS	IEPOX-derived organic sulfates	1E-10	3.60	216.2	1.947	
AIMGA	2-methylglyceric acid (2-MG)	1E-10	2.50	120.1	1.067	
AIMOS	MPAN-derived organic nitrates	1E-10	4.17	200.16	2.403	
ADIM	Dimers	1E-10	2.07	248.23	0.723	
AISO1	Semi-volatile isoprene SOA	116.01	2.20	132.0	0.827	
AISO2		0.617	2.23	133.0	0.857	
AISOPNN	Semi-volatile SOA from isoprene dinitrates produced from NO_3 reaction	8.9	3.80	226.0	2.107	Pye et al. (2015)
AMT1	Monoterpene SOA from OH/O_3-initiated oxidation	0.01	1.67	300.0	0.4	Xu et al. (2018)
AMT2		0.1	1.67	200.0	0.4	
AMT3		1	1.72	186.0	0.444	
AMT4		10	1.53	184.0	0.3	
AMT5		100	1.57	170.0	0.333	
AMT6		1000	1.40	168.0	0.2	
AMTNO3	Semi-volatile SOA from	12.0	1.90	231.0	0.587	Pye et al. (2015)

	monoterpene nitrates (excluding α-pinene)					
AMTHYD	Nonvolatile organic hydrolysis product of MTNO3[b] and ISOPNN[c]	1E-10	1.54	186.0	0.299	
ASQT	Sesquiterpene SOA	24.984	1.52	273.0	0.283	Carlton et al. (2010); Pye et al. (2017)
AOLGB	oligomers derived from BSOA	1E-10	2.10	248.0	0.747	Carlton et al. (2010); Pye et al. (2017)
AGLY	OA from glyoxal and methylglyoxal uptake onto accumulation-mode particles	1E-10	2.13	66.4	0.771	Pye et al. (2015)
AORGC	OA from aqueous-phase oxidation of glyoxal and methylglyoxal in cloud droplets	1E-10	2.00	177.0	0.677	Carlton et al. (2008)
APNCOM	Non-carbon fraction of POA	1E-10	1.60	220.0	0.347	Simon and Bhave (2012)
APOC	Carbon fraction of POA					
ALVPO1		0.1	1.39	218.0	0.185	
ASVPO1		1	1.32	230.0	0.123	
ASVPO2		10	1.26	241.0	0.073	
ASVPO3		100	1.21	253.0	0.032	
AIVPO1	Semi-volatile	1000	1.17	266.0	0.00	Murphy et al. (2017)
ALVOO1	POA	0.01	2.27	136.0	0.886	
ALVOO2		0.1	2.06	136.0	0.711	
ASVOO1		1	1.88	135.0	0.567	
ASVOO2		10	1.73	135.0	0.477	
ASVOO3		100	1.60	134.0	0.345	

[a] The parameters were calculated based on the methodology in Qin et al. (2021).

[b] MTNO3: Monoterpene-derived organic nitrates.

[c] ISOPNN: Second generation isoprene dinitrate from NO_3 reaction

.

Table S8 OA surrogate species in the 2D-VBS and their physicochemical properties at 298 K (Zhao et al., 2015; Chang et al., 2022), including saturated vapor pressure (C_0^*), organic matter to organic carbon ratio (OM/OC), molecular weight ($\tilde{M}$), and oxygen to carbon ratio (O/C).

Species	C_0^*	OM/OC	$\tilde{M}$	O/C
AM120	0.01	3.667	152.30	2.0
A0020	1	3.667	141.00	2.0
A0120	10	3.667	129.70	2.0
A0220	100	3.667	118.50	2.0
A0320	1000	3.667	107.20	2.0
A0420	1.0E+04	3.667	95.90	2.0
A0520	1.0E+05	3.667	84.60	2.0
A0620	1.0E+06	3.667	73.30	2.0
A0720	1.0E+07	3.667	62.10	2.0
AM115	0.01	3.041	161.60	1.5
A0015	1	3.041	149.60	1.5
A0115	10	3.041	137.60	1.5
A0215	100	3.041	125.70	1.5
A0315	1000	3.041	113.70	1.5
A0415	1.0E+04	3.041	101.70	1.5
A0515	1.0E+05	3.041	89.80	1.5
A0615	1.0E+06	3.041	77.80	1.5
A0715	1.0E+07	3.041	65.80	1.5
AM110	0.01	2.417	178.00	1.0
A0010	1	2.417	164.80	1.0
A0110	10	2.417	151.60	1.0
A0210	100	2.417	138.40	1.0
A0310	1000	2.417	125.20	1.0
A0410	1.0E+04	2.417	112.00	1.0
A0510	1.0E+05	2.417	98.90	1.0
A0610	1.0E+06	2.417	85.70	1.0
A0710	1.0E+07	2.417	72.50	1.0
AM107	0.01	2.042	195.70	0.7
A0007	1	2.042	181.20	0.7
A0107	10	2.042	166.70	0.7
A0207	100	2.042	152.20	0.7
A0307	1000	2.042	137.70	0.7

A0407	1.0E+04	2.042	123.20	0.7
A0507	1.0E+05	2.042	108.70	0.7
A0607	1.0E+06	2.042	94.20	0.7
A0707	1.0E+07	2.042	79.70	0.7
AM104	0.01	1.667	228.80	0.4
A0004	1	1.667	211.90	0.4
A0104	10	1.667	194.90	0.4
A0204	100	1.667	178.00	0.4
A0304	1000	1.667	161.00	0.4
A0404	1.0E+04	1.667	144.10	0.4
A0504	1.0E+05	1.667	127.10	0.4
A0604	1.0E+06	1.667	110.20	0.4
A0704	1.0E+07	1.667	93.20	0.4
AM102	0.01	1.417	273.20	0.2
A0002	1	1.417	253.00	0.2
A0102	10	1.417	232.70	0.2
A0202	100	1.417	212.50	0.2
A0302	1000	1.417	192.30	0.2
A0402	1.0E+04	1.417	172.00	0.2
A0502	1.0E+05	1.417	151.80	0.2
A0602	1.0E+06	1.417	131.50	0.2
A0702	1.0E+07	1.417	111.30	0.2
AM101	0.01	1.292	312.30	0.1
A0001	1	1.292	289.20	0.1
A0101	10	1.292	266.00	0.1
A0201	100	1.292	242.90	0.1
A0301	1000	1.292	219.80	0.1
A0401	1.0E+04	1.292	196.60	0.1
A0501	1.0E+05	1.292	173.50	0.1
A0601	1.0E+06	1.292	150.40	0.1
A0701	1.0E+07	1.292	127.20	0.1
AM100	0.01	1.167	378.00	0.0
A0000	1	1.167	350.00	0.0
A0100	10	1.167	322.00	0.0
A0200	100	1.167	294.00	0.0
A0300	1000	1.167	266.00	0.0
A0400	1.0E+04	1.167	238.00	0.0

A0500	1.0E+05	1.167	210.00	0.0
A0600	1.0E+06	1.167	182.00	0.0
A0700	1.0E+07	1.167	154.00	0.0
ADIM	1E-10	2.07	248.23	0.723
AGLY	1E-10	2.13	66.4	0.771
AIEOS	1E-10	3.60	216.2	1.947
AIETET	1E-10	2.27	136.15	0.833
AIMGA	1E-10	2.50	120.1	1.067
AIMOS	1E-10	4.17	200.16	2.403
AISO1	116.01	2.20	132.0	0.827
AISO2	0.617	2.23	133.0	0.857
AISO3	1E-10	2.80	168.2	1.307
AISOPNN	8.9	3.80	226.0	2.107
AMTNO3	12.0	1.90	231.0	0.587
AMTHYD	1E-10	1.54	186.0	0.299
AOLGB	1E-10	2.10	248.0	0.747

Note: While ASOA, BSOA, and POA are separately represented in the model, species with identical volatility and O/C are assumed to share physicochemical properties and are not listed individually in this table.

Table S9 Contribution of SOA to OA in different simulations.

Site	Case	SIM	OBS
DY	1D-VBS	59%	72%
	1D-VBS_E	62%	
	1D-VBS_EY	67%	
	2D-VBS	82%	
GZ	1D-VBS	78%	64%
	1D-VBS_E	72%	
	1D-VBS_EY	77%	
	2D-VBS	84%	

Table S10 CMAQ performance in hourly OA, SOA and POA simulations.

Site	Pollu-tant	Case	NMB	NME	r
DY	OA	1D-VBS	-0.67	0.67	0.87
		1D-VBS_E	-0.37	0.39	0.85
		1D-VBS_EY	-0.27	0.36	0.84
		2D-VBS	-0.24	0.38	0.83
	SOA	1D-VBS	-0.72	0.72	0.78
		1D-VBS_E	-0.45	0.49	0.74
		1D-VBS_EY	-0.30	0.43	0.75
		2D-VBS	-0.11	0.41	0.75
	POA	1D-VBS	-0.55	0.55	0.80
		1D-VBS_E	-0.20	0.30	0.84
		1D-VBS_EY	-0.21	0.30	0.84
		2D-VBS	-0.54	0.54	0.86
GZ	OA	1D-VBS	-0.72	0.72	0.34
		1D-VBS_E	-0.44	0.48	0.33
		1D-VBS_EY	-0.34	0.41	0.33
		2D-VBS	-0.24	0.36	0.39
	SOA	1D-VBS	-0.71	0.71	0.46
		1D-VBS_E	-0.47	0.48	0.44
		1D-VBS_EY	-0.33	0.39	0.43
		2D-VBS	-0.14	0.33	0.43
	POA	1D-VBS	-0.76	0.76	0.05
		1D-VBS_E	-0.40	0.60	0.06
		1D-VBS_EY	-0.41	0.61	0.07
		2D-VBS	-0.53	0.60	0.35

Supplementary Figures

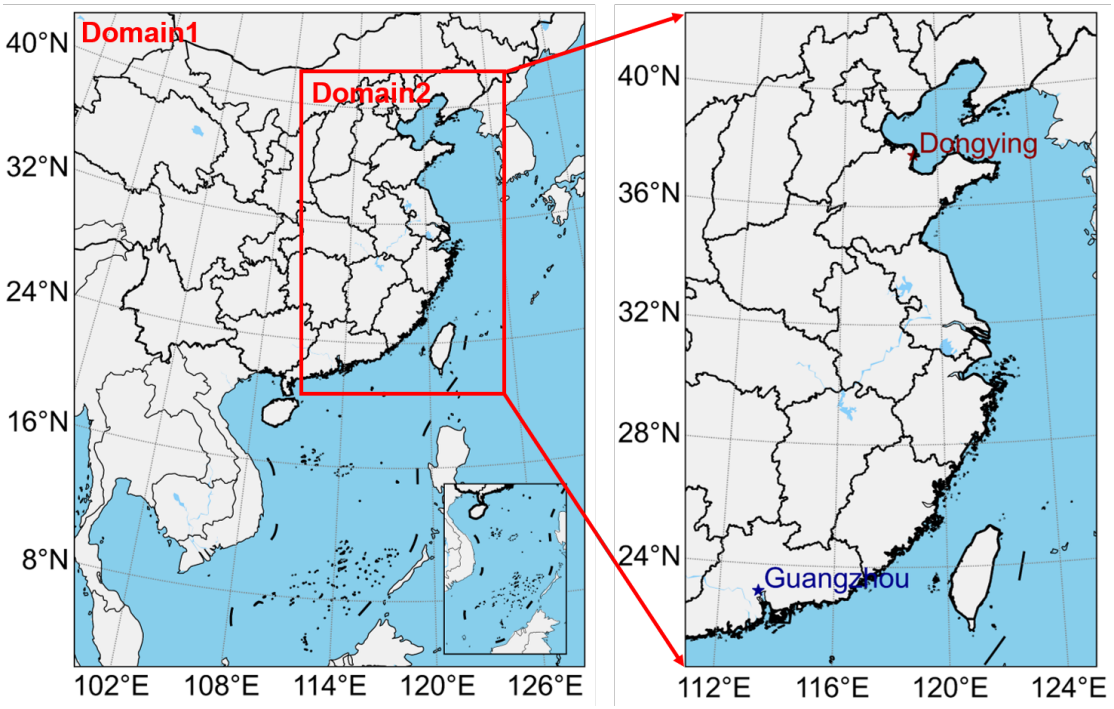

Figure S1 Modeling domains and locations of observational sites Dongying (DY) and Guangzhou (GZ).

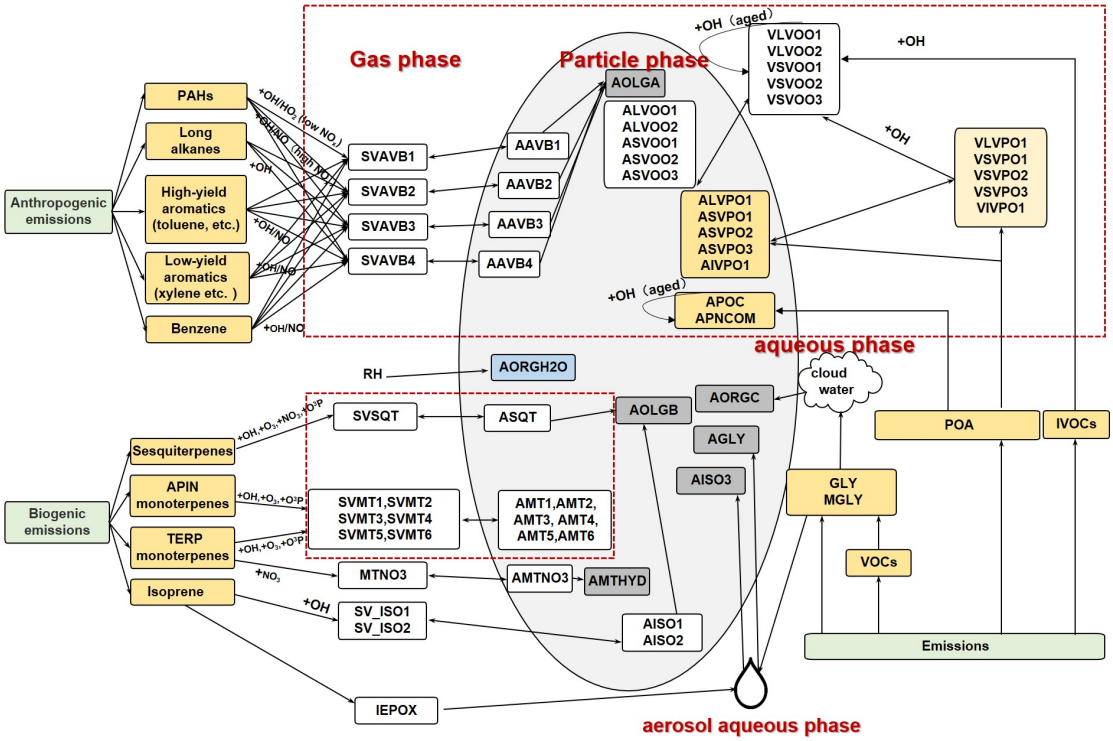

104

105

106 **Figure S2** Organic aerosol treatment in CMAQv5.3-aero7i. Species in grey boxes are assumed
107 to be non-volatile. The schematic diagram is adapted from Fig.3 in Pye et al. (2017). Boxes
108 outlined in red dashed lines indicate that SOA was represented within the 1D-VBS framework
109 in the aero7i module, which is replaced by the 2D-VBS scheme in CMAQv5.4. SOA derived
110 from isoprene, glyoxal, methylglyoxal, and monoterpenes+NO_3 was treated consistently in both
111 the 1D-VBS and 2D-VBS simulations.

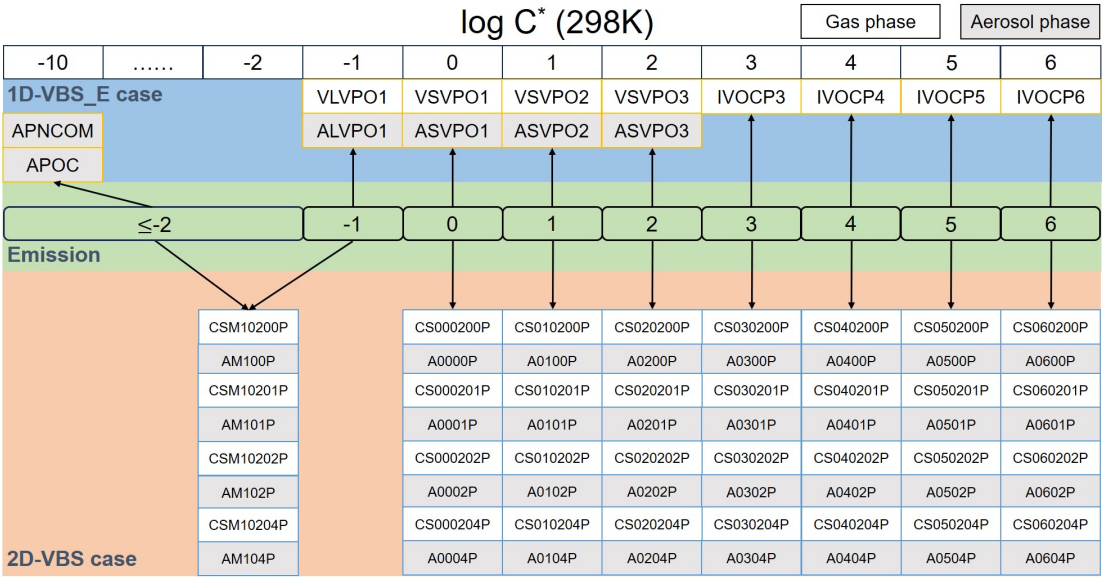

Figure S3 Volatility distribution of L/S/IVOC emissions in the 1D-VBS_Y and 2D-VBS simulations. The green area shows L/S/IVOC emission estimates. The blue and orange areas represent allocation of these emissions across volatility bins in the 1D-VBS_E and 2D-VBS simulations, respectively. Grey boxes denote aerosol phase, and white boxes indicate gas phase.

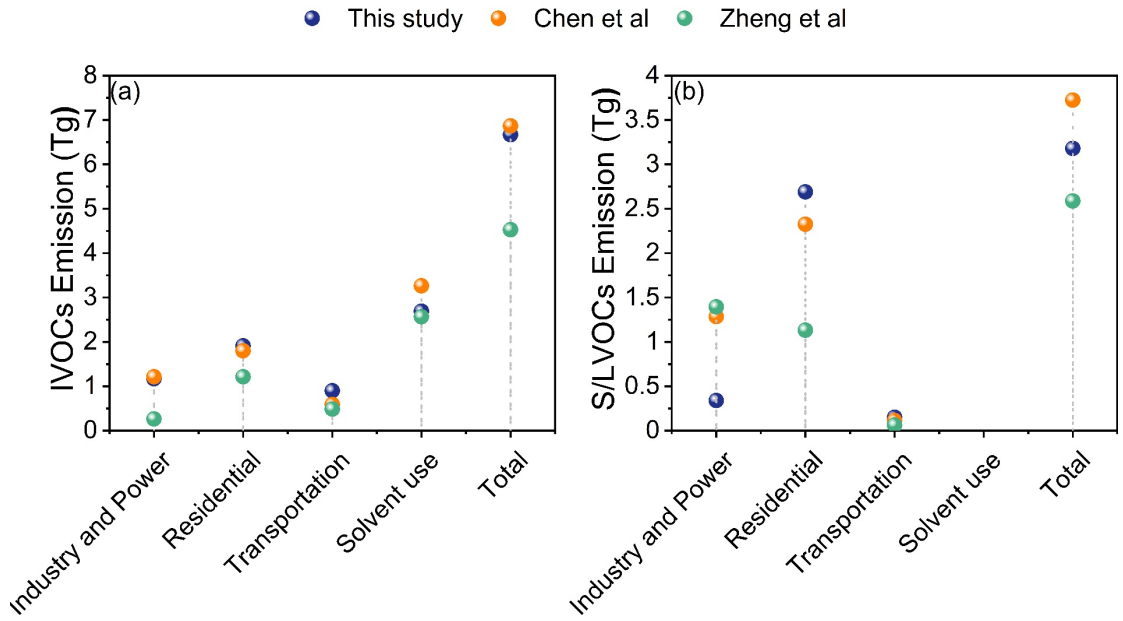

Figure S4 Comparison of annual emissions of (a) IVOC and (b) S/LVOC emissions in China in 2018 from this study with the estimates from Chen et al. (2024) and Zheng et al. (2023).

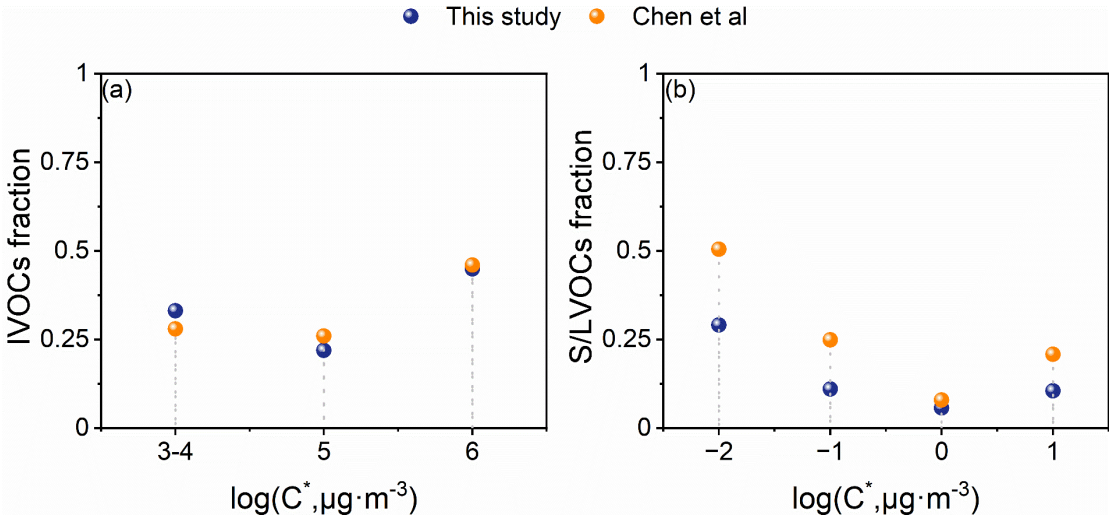

123

124 **Figure S5** Comparison of the volatility distributions of (a) IVOC and (b) S/LVOC emissions
125 across all volatility bins in China in 2018 between this study and estimates from Chen et al.
126 (2024).

127

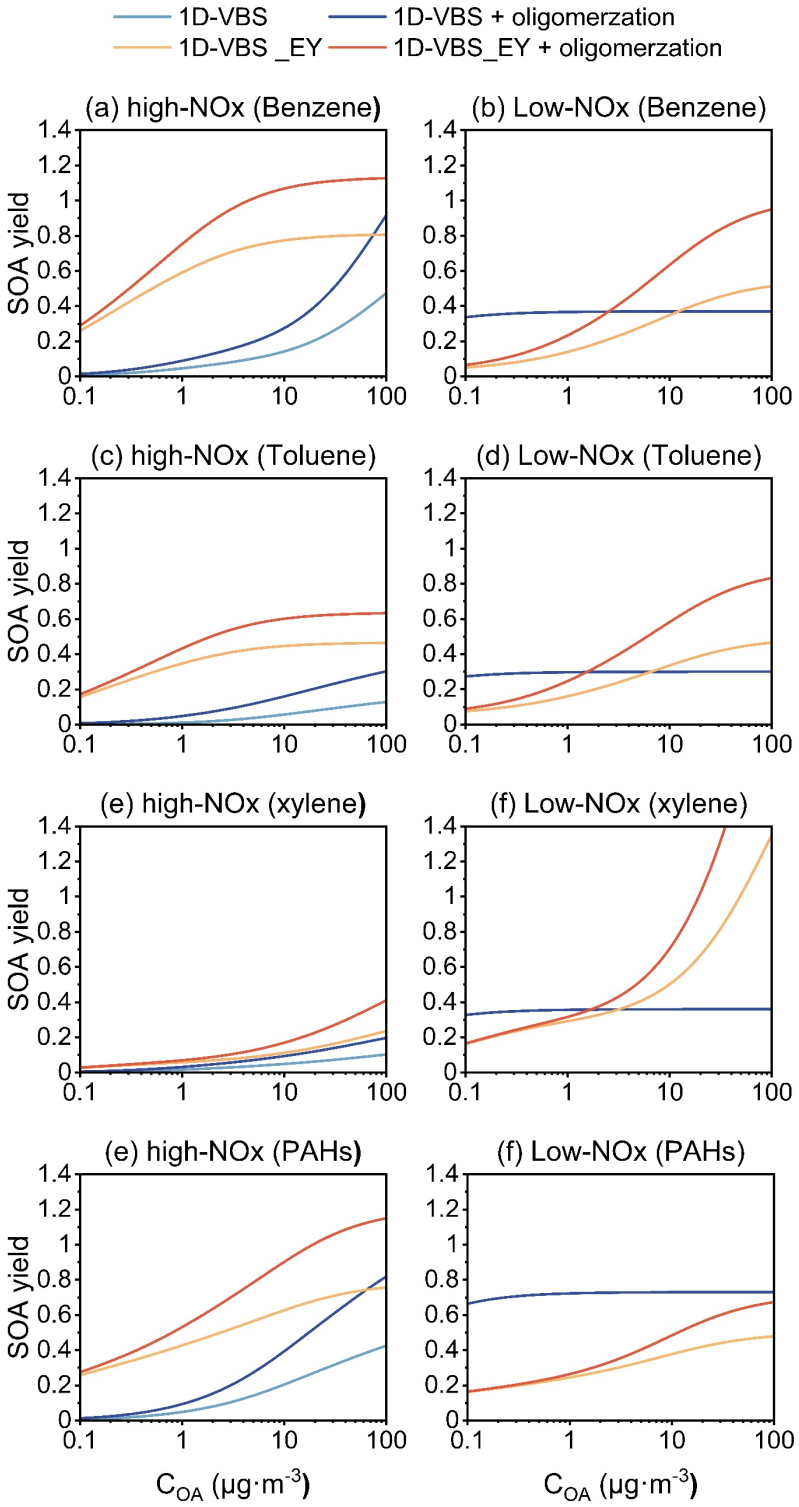

Figure S6 SOA mass yield from aromatic hydrocarbons (a, b: benzene; c, d: toluene; e, f: xylene; g, h: PAHs) under high-NOx and low-NOx conditions.

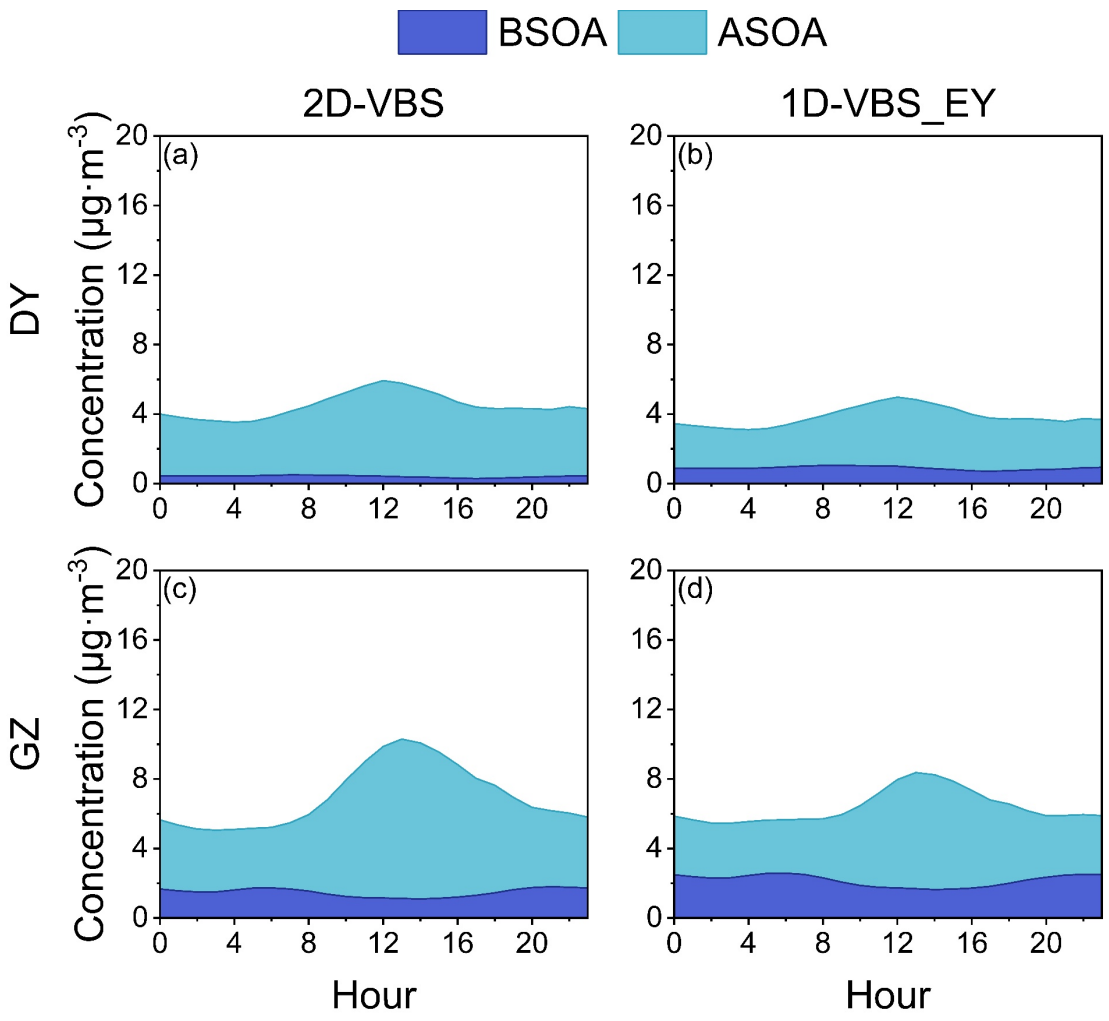

132

133 **Figure S7** Diurnal variations of SOA compositions (ASOA and BSOA) from 1D-VBS_EY and

134 2D-VBS simulations in DY (a-b) and GZ (c-d).

135

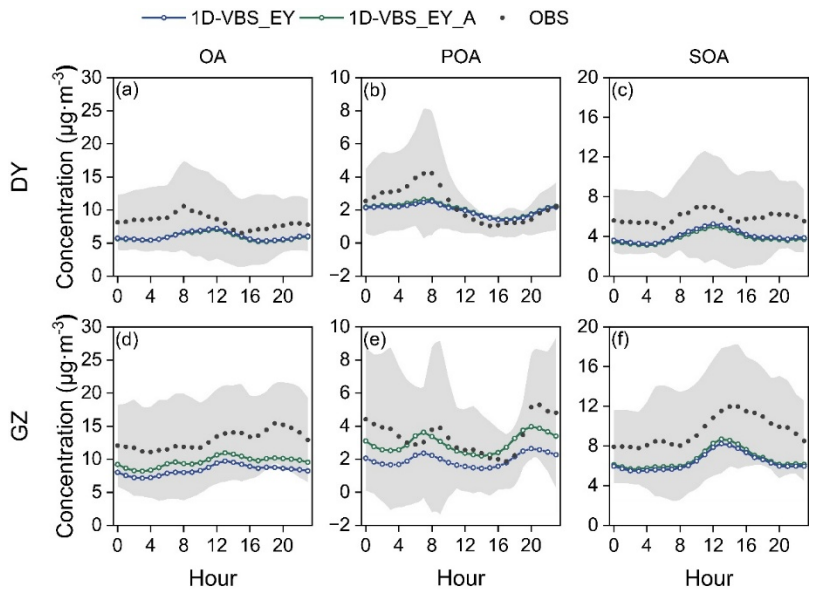

136

137 **Figure S8** Simulated diurnal variations of OA, POA, and SOA at DY (a–c) and GZ (d–f) com-
138 pared with observations. Blue lines represent the 1D-VBS_EY case, and green lines represent
139 the sensitivity case (1D-VBS_EY_A) with scaled POA emissions. Black dots denote observa-
140 tions. The light grey shading indicates the standard deviations (±1σ) from the mean concentra-
141 tions in the observations.

142

143

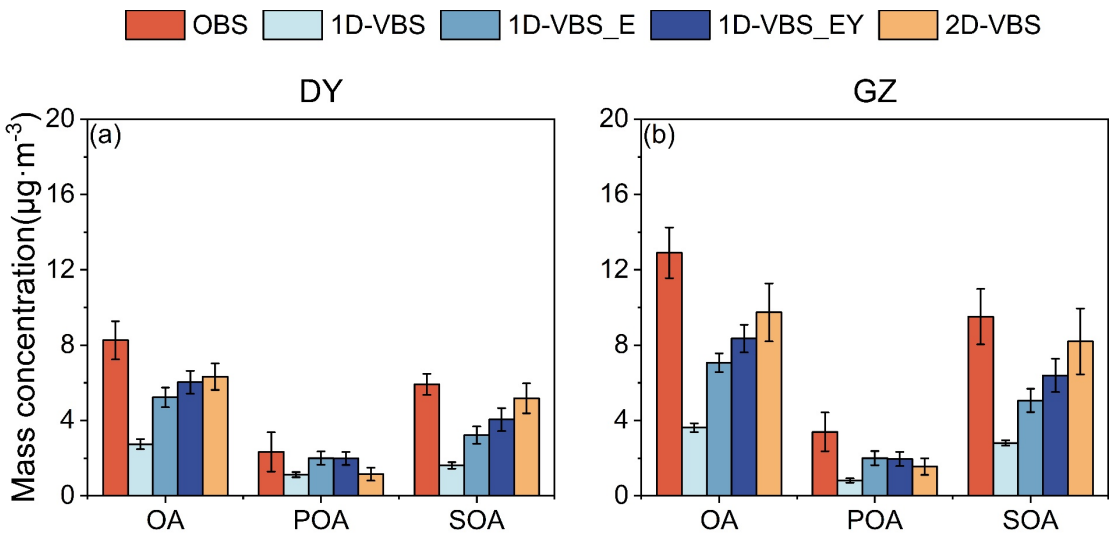

144

145 **Figure S9** Period-averaged mass concentrations of modeled and observed OA, POA, and SOA

146 in DY (a) and GZ (b), with BBOA and COA excluded from the OA and POA observations.

147

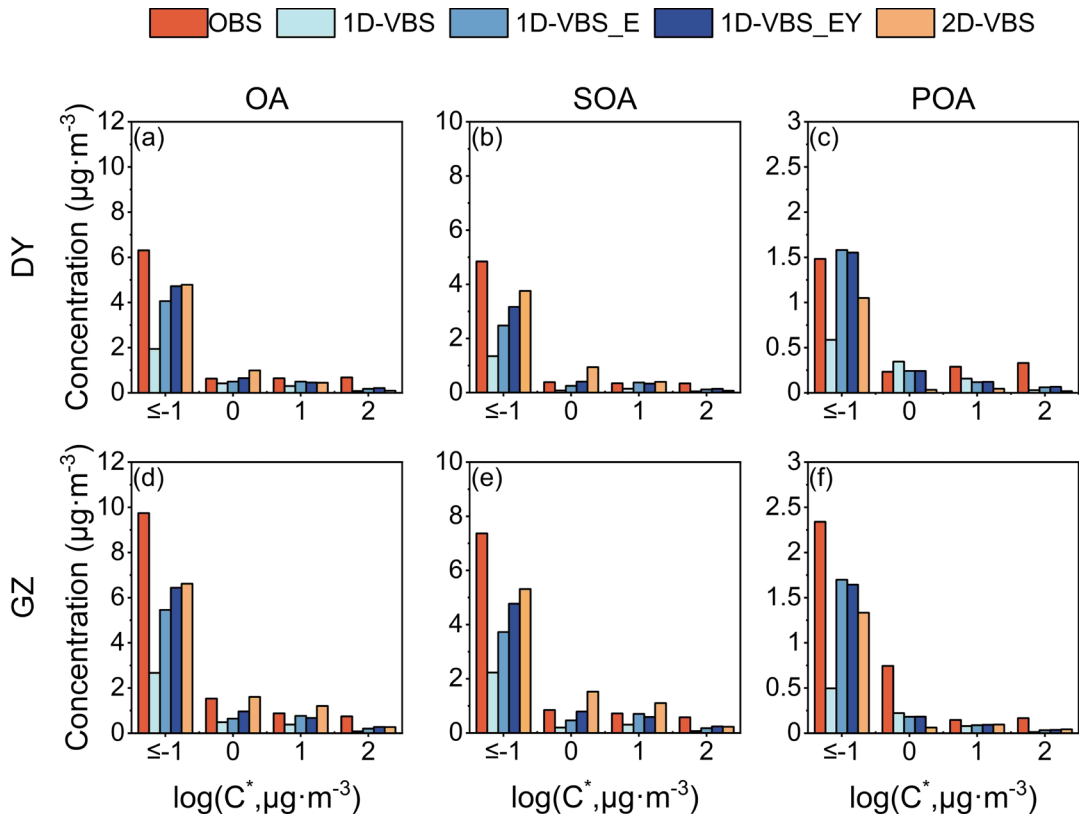

Figure S10 Simulated mass concentrations of OA, POA, and SOA across volatility bins with C^* ranging from $<10^{-1}$ to 10^2 μg m^{-3}, compared to observations in DY (a-c) and GZ (d-f).

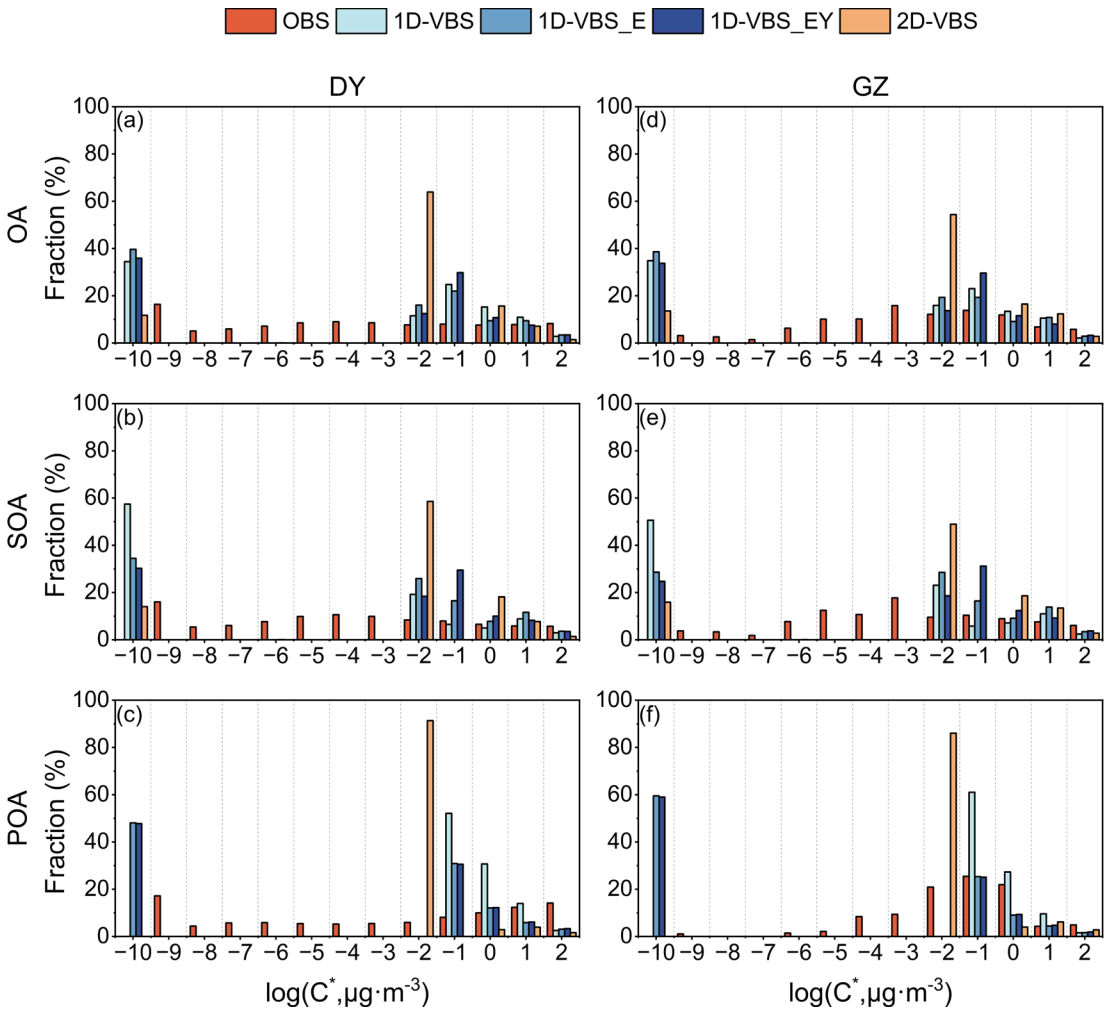

Figure S11 Simulated OA, POA, and SOA volatility distributions across volatility bins with C^* ranging from 10^{-10} to 10^{2} μg m^{-3}, compared to the observations in DY (a-c) and GZ (d-f).

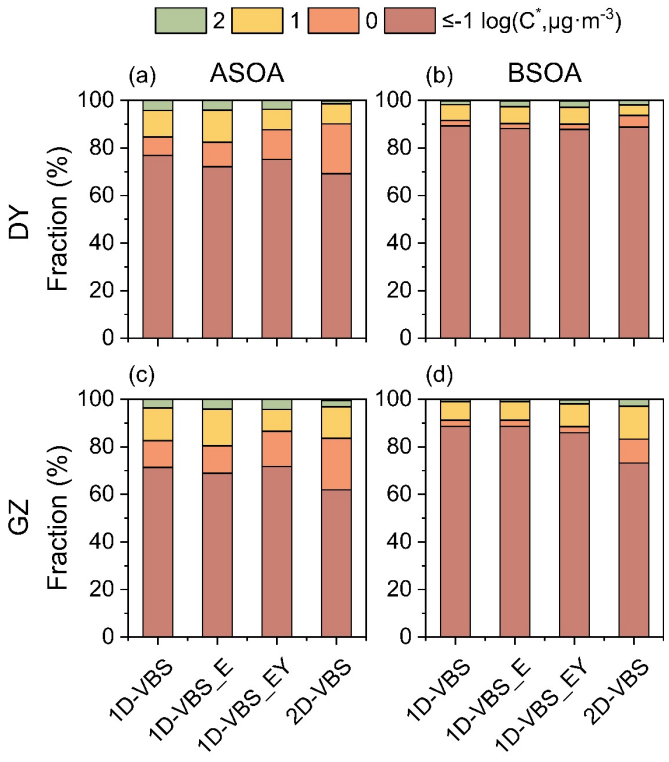

157

158 **Figure S12** Simulated volatility distributions of BSOA and ASOA in DY (a-b) and GZ (c-d).

159

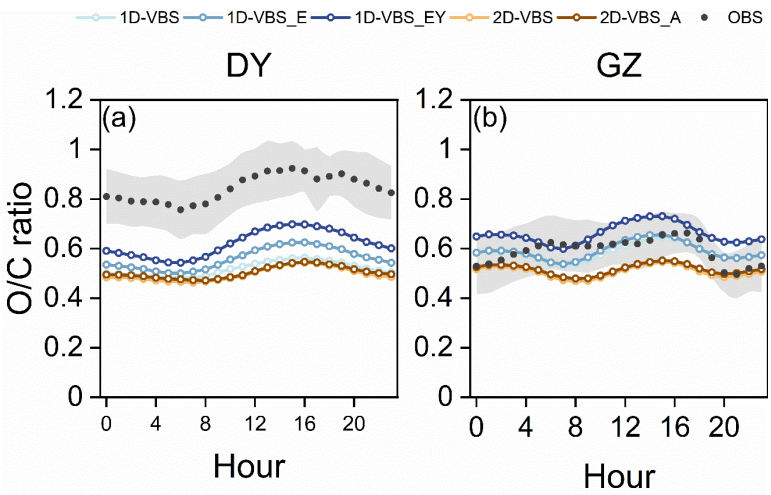

Figure S13 Simulated diurnal variations of OA O/C ratios compared to observations in DY (a) and GZ (b).

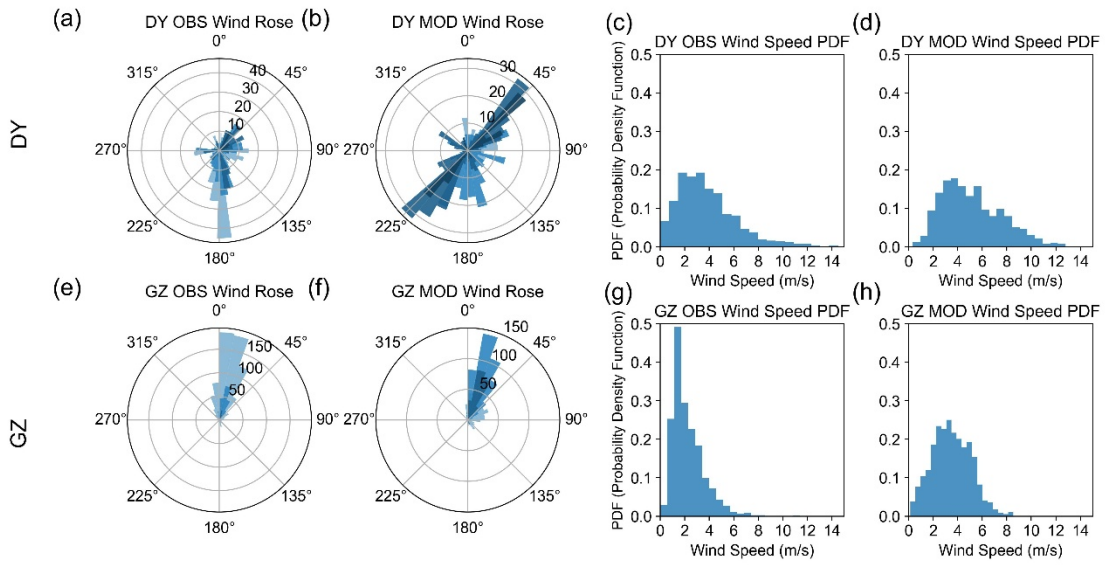

165

166 **Figure S14** Observed and simulated wind roses and wind speed probability density functions

167 (PDFs) at the DY (a–d) and GZ (e–h) sites.

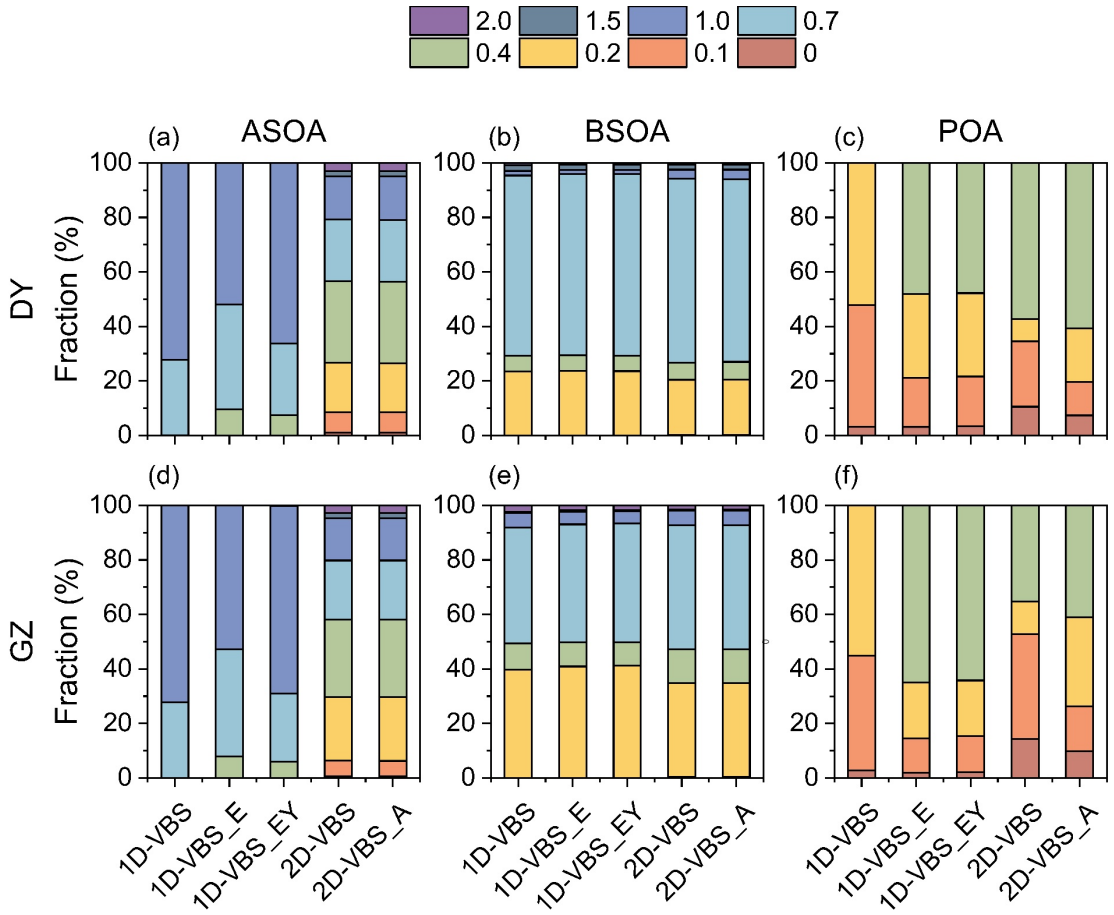

168

169 **Figure S15** Mass contributions of ASOA, BSOA and POA across O/C bins in DY (a-c) and

170 GZ(d-f). The numbers in the legends represent median O/C values.

171

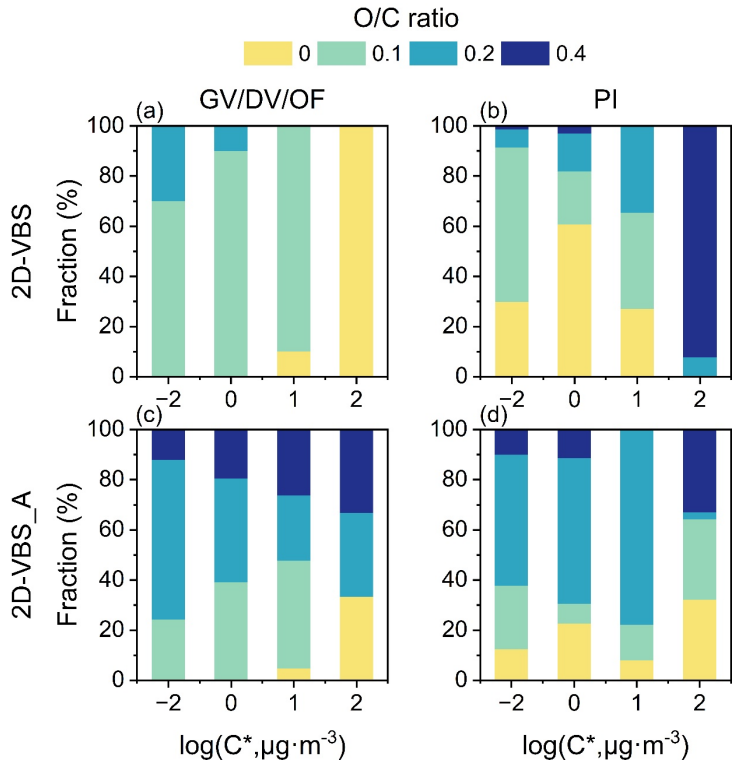

172

173 **Figure S16** O/C distributions of L/SVOC emissions from gasoline/diesel vehicles or off-road
174 mobile sources (GV/DV/OF), and power plants or industrial sources (PI) in the 2D-VBS sim-
175 ulation (a–b) and the 2D-VBS_A simulation (c–d).

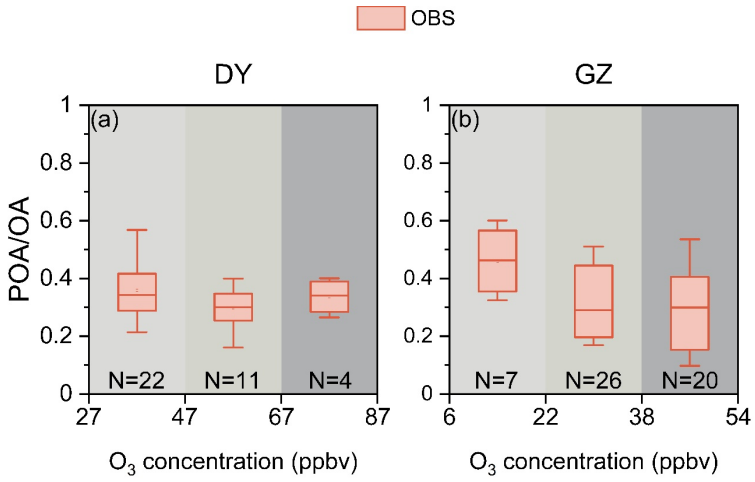

Figure S17 Variation of POA/OA ratios with daily average ozone concentrations in the observations in DY (a) and GZ (b). N denotes the sample size of POA/OA ratios within each ozone interval.

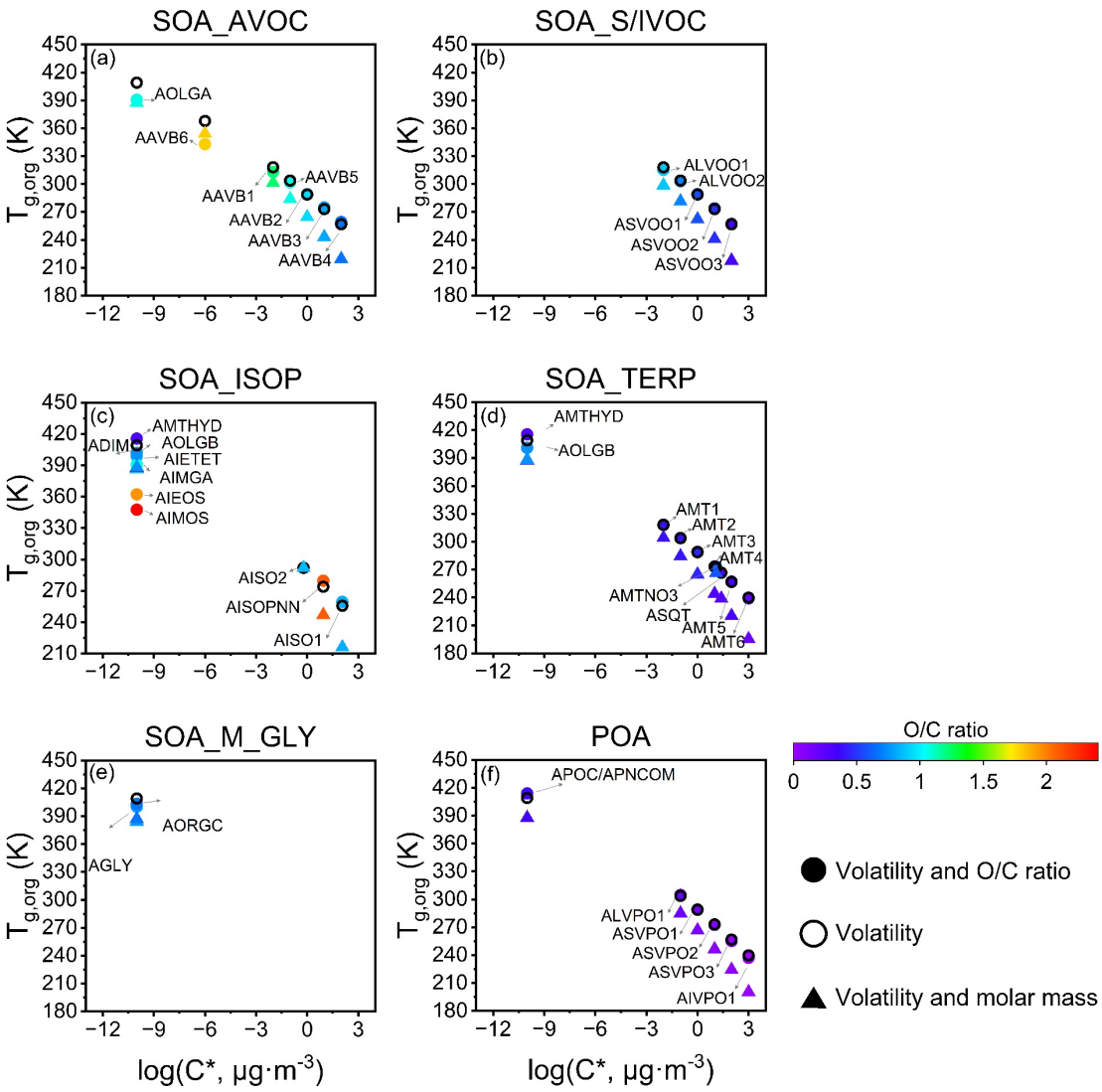

Figure S18 Estimated T_g values for OA surrogate species. Solid circles represent $T_{g,org}$ calculated using both volatility and O/C ratios, with colors indicating the O/C ratio, while open circles represent $T_{g,org}$ calculated using volatility alone and solid triangles represent $T_{g,org}$ calculated using volatility and molar mass (see Table S6 for a more detailed description of the CMAQ OA species).

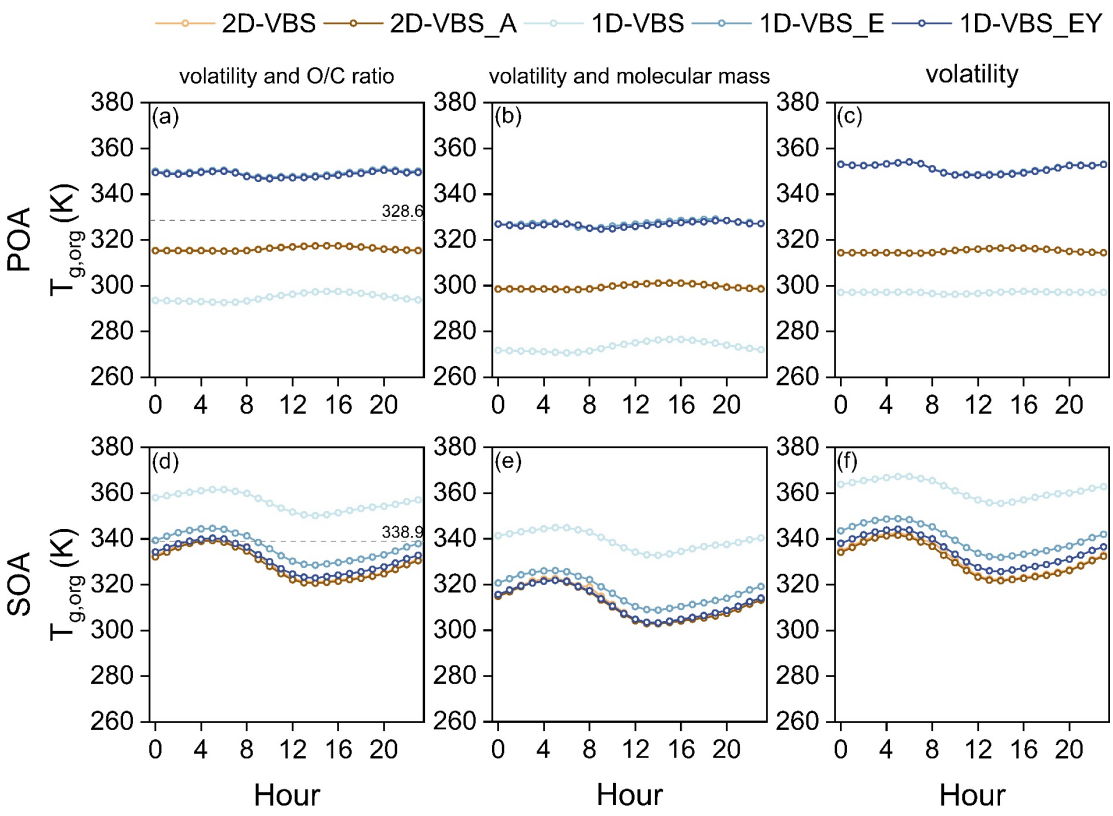

Figure S19 Comparison of simulated diurnal variations of POA and SOA $T_{g,org}$ with estimates based on observations in DY. $T_{g,org}$ values were estimated using both volatility and O/C ratios (a)(d), volatility and molecular masses (b)(e), and volatility only (c)(f), respectively.

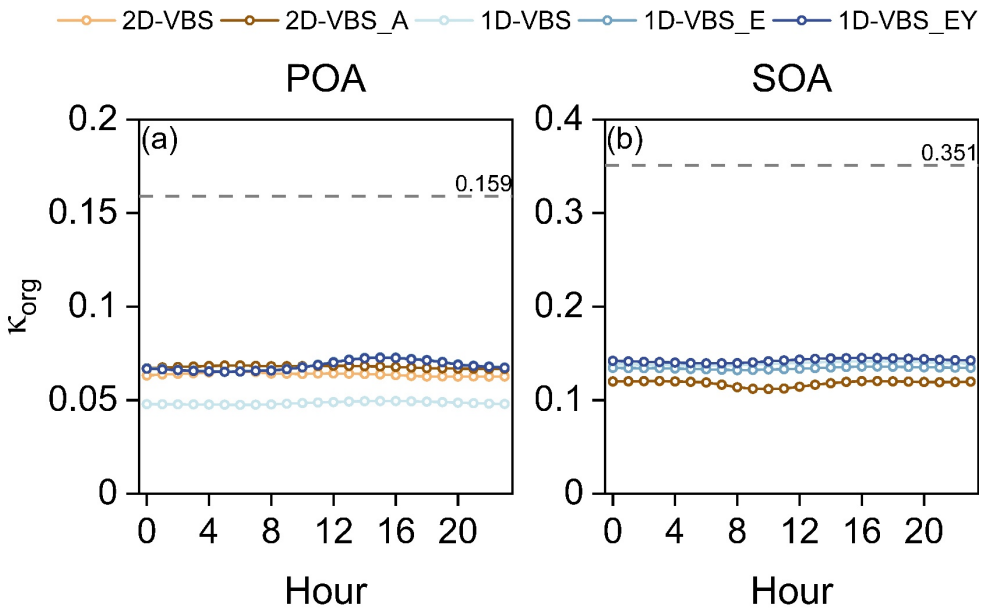

Figure S20 Diurnal variation of (a) POA and (b) SOA κ_{org}, predicted as a function of OM/OC, with the grey dashed line representing the κ_{org} value derived from observations, estimated as a function of f_{44} (i.e., the fraction of m/z 44 signal in total organic signals).

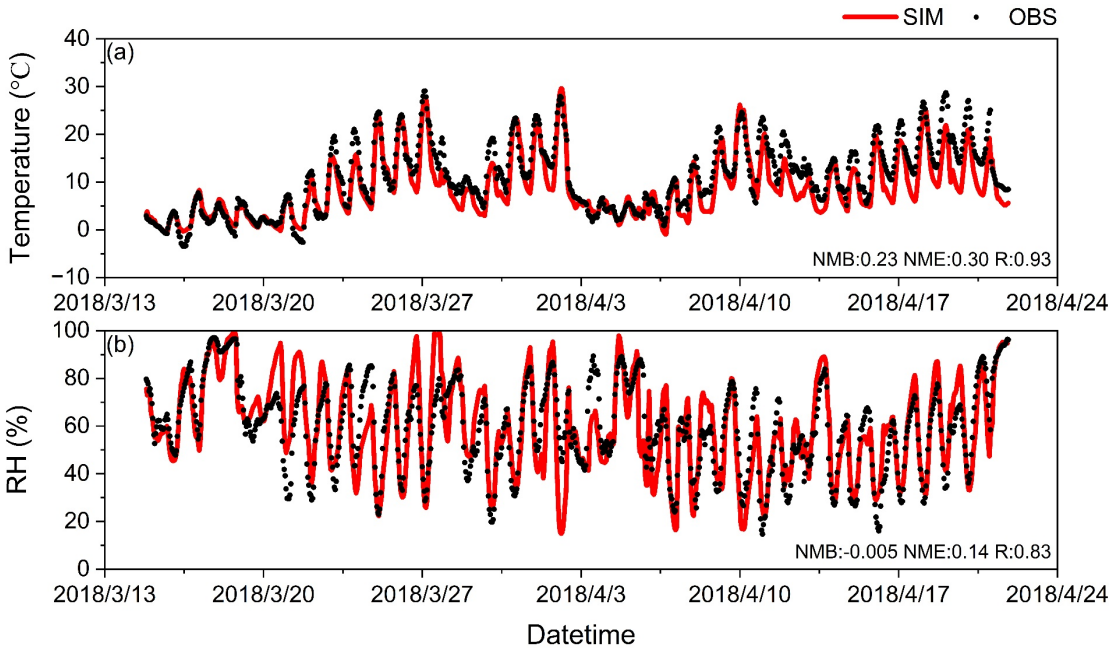

Figure S21 Time series of (a) temperature (T) and (b) relative humidity (RH) at the DY site.

Supplementary References

An, J., Huang, C., Huang, D., Qin, M., Liu, H., Yan, R., Qiao, L., Zhou, M., Li, Y., Zhu, S., Wang, Q., and Wang, H.: Sources of organic aerosols in eastern China: a modeling study with high-resolution intermediate-volatility and semivolatile organic compound emissions, Atmos. Chem. Phys., 23, 323-344, https://doi.org/10.5194/acp-23-323-2023, 2023.

Bilsback, K. R., He, Y., Cappa, C. D., Chang, R. Y.-W., Croft, B., Martin, R. V., Ng, N. L., Seinfeld, J. H., Pierce, J. R., and Jathar, S. H.: Vapors Are Lost to Walls, Not to Particles on the Wall: Artifact-Corrected Parameters from Chamber Experiments and Implications for Global Secondary Organic Aerosol, Environ Sci Technol, 57, 53-63, https://doi.org/10.1021/acs.est.2c03967, 2023.

Carlton, A. G., Turpin, B. J., Altieri, K. E., Seitzinger, S. P., Mathur, R., Roselle, S. J., and Weber, R. J.: CMAQ Model Performance Enhanced When In-Cloud Secondary Organic Aerosol is Included: Comparisons of Organic Carbon Predictions with Measurements, Environ. Sci. Technol., 42, 8798-8802, https://doi.org/10.1021/es801192n, 2008.

Carlton, A. G., Bhave, P. V., Napelenok, S. L., Edney, E. O., Sarwar, G., Pinder, R. W., Pouliot, G. A., and Houyoux, M.: Model representation of secondary organic aerosol in CMAQv4.7, Environ. Sci. Technol., 44, 8553-8560, https://doi.org/10.1021/es100636q, 2010.

Chang, X., Zhao, B., Zheng, H., Wang, S., Cai, S., Guo, F., Gui, P., Huang, G., Wu, D., Han, L., Xing, J., Man, H., Hu, R., Liang, C., Xu, Q., Qiu, X., Ding, D., Liu, K., Han, R., Robinson, A. L., and Donahue, N. M.: Full-volatility emission framework corrects missing and underestimated secondary organic aerosol sources, One Earth, 5, 403-412, https://doi.org/10.1016/j.oneear.2022.03.015, 2022.

Che, H., Shen, X., Yao, Z., Wu, B., Gou, R., Hao, X., Cao, X., Li, X., Zhang, H., Wang, S., and Chen, Z.: Real-world emission characteristics and inventory of volatile organic compounds originating from construction and agricultural machinery, Sci. Total Environ., 894, 164993, https://doi.org/10.1016/j.scitotenv.2023.164993, 2023.

Chen, Q., Miao, R., Geng, G., Shrivastava, M., Dao, X., Xu, B., Sun, J., Zhang, X., Liu, M., Tang, G., Tang, Q., Hu, H., Huang, R.-J., Wang, H., Zheng, Y., Qin, Y., Guo, S., Hu, M., and Zhu, T.: Widespread 2013-2020 decreases and reduction challenges of organic aerosol in China, Nat. Commun., 15, 4465, https://doi.org/10.1038/s41467-024-48902-0, 2024.

Chen, W., Ye, Y., Hu, W., Zhou, H., Pan, T., Wang, Y., Song, W., Song, Q., Ye, C., Wang, C., Wang, B., Huang, S., Yuan, B., Zhu, M., Lian, X., Zhang, G., Bi, X., Jiang, F., Liu, J., Canonaco, F., Prevot, A. S. H., Shao, M., and Wang, X.: Real‐Time Characterization of Aerosol Compositions, Sources, and Aging Processes in Guangzhou During PRIDE‐GBA 2018 Campaign, J. Geophys. Res., 126, e2021JD035114, https://doi.org/10.1029/2021JD035114, 2021.

Emery, C. and Tai, E.: Enhanced Meteorological Modeling and Performance Evaluation for Two Texas Ozone Episodes,

Emery, C., Liu, Z., Russell, A. G., Odman, M. T., Yarwood, G., and Kumar, N.: Recommendations on statistics and benchmarks to assess photochemical model performance, J. Air Waste Manag. Assoc., 67, 582-598, https://doi.org/10.1080/10962247.2016.1265027, 2017.

Feng, T., Wang, Y., Hu, W., Zhu, M., Song, W., Chen, W., Sang, Y., Fang, Z., Deng, W., Fang, H., Yu, X., Wu, C., Yuan, B., Huang, S., Shao, M., Huang, X., He, L., Lee, Y. R., Huey, L. G., Canonaco, F., Prevot, A. S. H., and Wang, X.: Impact of aging on the sources, volatility, and viscosity of organic aerosols in Chinese outflows, Atmos. Chem. Phys., 23, 611-636, https://doi.org/10.5194/acp-23-611-2023, 2023.

Ge, X., Li, L., Chen, Y., Chen, H., Wu, D., Wang, J., Xie, X., Ge, S., Ye, Z., Xu, J., and Chen, M.: Aerosol

characteristics and sources in Yangzhou, China resolved by offline aerosol mass spectrometry and other techniques, Environmental Pollution, 225, 74-85, https://doi.org/10.1016/j.envpol.2017.03.044, 2017.
Gu, C., Cui, S., Ge, X., Wang, Z., Chen, M., Qian, Z., Liu, Z., Wang, X., and Zhang, Y.: Chemical composition, sources and optical properties of nitrated aromatic compounds in fine particulate matter during winter foggy days in Nanjing, China, Environ.Res., 212, 113255, https://doi.org/10.1016/j.envres.2022.113255, 2022.
Huang, C., Hu, Q., Li, Y., Tian, J., Ma, Y., Zhao, Y., Feng, J., An, J., Qiao, L., Wang, H., Jing, S., Huang, D., Lou, S., Zhou, M., Zhu, S., Tao, S., and Li, L.: Intermediate Volatility Organic Compound Emissions from a Large Cargo Vessel Operated under Real-World Conditions, Environ. Sci. Technol., 52, 12934-12942, https://doi.org/10.1021/acs.est.8b04418, 2018.
Kohl, I., Bachmann, L., Hallbrucker, A., Mayer, E., and Loerting, T.: Liquid-like relaxation in hyperquenched water at≤ 140 K, Physical Chemistry Chemical Physics, 7, 3210-3220, 2005.
Li, K., Chen, L., White, S. J., Zheng, X., Lv, B., Lin, C., Bao, Z., Wu, X., Gao, X., Ying, F., Shen, J., Azzi, M., and Cen, K.: Chemical characteristics and sources of PM1 during the 2016 summer in Hangzhou, Environmental Pollution, 232, 42-54, https://doi.org/10.1016/j.envpol.2017.09.016, 2018.
Lu, Q. Y., Murphy, B. N., Qin, M. M., Adams, P., Zhao, Y. L., Pye, H. O. T., Efstathiou, C., Allen, C., and Robinson, A. L.: Simulation of organic aerosol formation during the CalNex study: updated mobile emissions and secondary organic aerosol parameterization for intermediate-volatility organic compounds, Atmos. Chem. Phys., 20, 4313-4332, https://doi.org/10.5194/acp-20-4313-2020, 2020.
McDonald, B., de Gouw, J., Gilman, J., Jathar, S., Akherati, A., Cappa, C., Jimenez, J., Lee-Taylor, J., Hayes, P., McKeen, S., Cui, Y., Kim, S.-W., Gentner, D., Isaacman-VanWertz, G., Goldstein, A., Harley, R., Frost, G., Roberts, J., Ryerson, T., and Trainer, M.: Volatile chemical products emerging as largest petrochemical source of urban organic emissions, Science (New York, N.Y.), 359, 760-764, https://doi.org/10.1126/science.aaq0524, 2018.
Murphy, B. N., Woody, M. C., Jimenez, J. L., Carlton, A. M. G., Hayes, P. L., Liu, S., Ng, N. L., Russell, L. M., Setyan, A., Xu, L., Young, J., Zaveri, R. A., Zhang, Q., and Pye, H. O. T.: Semivolatile POA and parameterized total combustion SOA in CMAQv5.2: impacts on source strength and partitioning, Atmos. Chem. Phys., 17, 11107-11133, https://doi.org/10.5194/acp-17-11107-2017, 2017.
Pye, H. O. T., Luecken, D. J., Xu, L., Boyd, C. M., Ng, N. L., Baker, K. R., Ayres, B. R., Bash, J. O., Baumann, K., Carter, W. P. L., Edgerton, E., Fry, J. L., Hutzell, W. T., Schwede, D. B., and Shepson, P. B.: Modeling the Current and Future Roles of Particulate Organic Nitrates in the Southeastern United States, Environ. Sci. Technol., 49, 14195-14203, https://doi.org/10.1021/acs.est.5b03738, 2015.
Pye, H. O. T., Pinder, R. W., Piletic, I. R., Xie, Y., Capps, S. L., Lin, Y.-H., Surratt, J. D., Zhang, Z., Gold, A., Luecken, D. J., Hutzell, W. T., Jaoui, M., Offenberg, J. H., Kleindienst, T. E., Lewandowski, M., and Edney, E. O.: Epoxide Pathways Improve Model Predictions of Isoprene Markers and Reveal Key Role of Acidity in Aerosol Formation, Environ. Sci. Technol., 47, 11056-11064, https://doi.org/10.1021/es402106h, 2013.
Pye, H. O. T., Murphy, B. N., Xu, L., Ng, N. L., Carlton, A. G., Guo, H., Weber, R., Vasilakos, P., Appel, K. W., Budisulistiorini, S. H., Surratt, J. D., Nenes, A., Hu, W., Jimenez, J. L., Isaacman-VanWertz, G., Misztal, P. K., and Goldstein, A. H.: On the implications of aerosol liquid water and phase separation for organic aerosol mass, Atmos. Chem. Phys., 17, 343-369, 10.5194/acp-17-343-2017, 2017.
Qin, M., Murphy, B. N., Isaacs, K. K., McDonald, B. C., Lu, Q., McKeen, S. A., Koval, L., Robinson, A. L., Efstathiou, C., Allen, C., and Pye, H. O. T.: Criteria pollutant impacts of volatile chemical products informed by near-field modelling, Nature Sustainability, 4, 129-137, 2021.

Shen, X., Che, H., Lv, T., Wu, B., Cao, X., Li, X., Zhang, H., Hao, X., Zhou, Q., and Yao, Z.: Real-world emission characteristics of semivolatile/intermediate-volatility organic compounds originating from nonroad construction machinery in the working process, Sci. Total Environ., 858, 159970, https://doi.org/10.1016/j.scitotenv.2022.159970, 2023.

Simon, H. and Bhave, P. V.: Simulating the Degree of Oxidation in Atmospheric Organic Particles, Environmental Science & Technology, 46, 331-339, 10.1021/es202361w, 2012.

Tang, R., Lu, Q., Guo, S., Wang, H., Song, K., Yu, Y., Tan, R., Liu, K., Shen, R., Chen, S., Zeng, L., Jorga, S. D., Zhang, Z., Zhang, W., Shuai, S., and Robinson, A. L.: Measurement report: Distinct emissions and volatility distribution of intermediate-volatility organic compounds from on-road Chinese gasoline vehicles: implication of high secondary organic aerosol formation potential, Atmos. Chem. Phys., 21, 2569-2583, https://doi.org/10.5194/acp-21-2569-2021, 2021.

Xian, J., Cui, S., Chen, X., Wang, J., Xiong, Y., Gu, C., Wang, Y., Zhang, Y., Li, H., Wang, J., and Ge, X.: Online chemical characterization of atmospheric fine secondary aerosols and organic nitrates in summer Nanjing, China, Atmos. Res., 290, 106783, https://doi.org/10.1016/j.atmosres.2023.106783, 2023.

Xu, J., Liu, D., Wu, X., Vu, T. V., Zhang, Y., Fu, P., Sun, Y., Xu, W., Zheng, B., Harrison, R. M., and Shi, Z.: Source apportionment of fine organic carbon at an urban site of Beijing using a chemical mass balance model, Atmos. Chem. Phys., 21, 7321-7341, https://doi.org/10.5194/acp-21-7321-2021, 2021.

Xu, L., Pye, H. O. T., He, J., Chen, Y., Murphy, B. N., and Ng, N. L.: Experimental and model estimates of the contributions from biogenic monoterpenes and sesquiterpenes to secondary organic aerosol in the southeastern United States, Atmos. Chem. Phys., 18, 12613-12637, https://doi.org/10.5194/acp-18-12613-2018, 2018.

Zhang, Y., Zhang, X., Zhong, J., Sun, J., Shen, X., Zhang, Z., Xu, W., Wang, Y., Liang, L., Liu, Y., Hu, X., He, M., Pang, Y., Zhao, H., Ren, S., and Shi, Z.: On the fossil and non-fossil fuel sources of carbonaceous aerosol with radiocarbon and AMS-PMF methods during winter hazy days in a rural area of North China plain, Environ.Res., 208, 112672, https://doi.org/10.1016/j.envres.2021.112672, 2022.

Zhao, B., Wang, S., Donahue, N. M., Chuang, W., Hildebrandt Ruiz, L., Ng, N. L., Wang, Y., and Hao, J.: Evaluation of One-Dimensional and Two-Dimensional Volatility Basis Sets in Simulating the Aging of Secondary Organic Aerosol with Smog-Chamber Experiments, Environ. Sci. Technol., 49, 2245-2254, https://doi.org/10.1021/es5048914, 2015.

Zhao, J., Qi, L., Lv, Z., Wang, X., Deng, F., Zhang, Z., Luo, Z., Bie, P., He, K., and Liu, H.: An updated comprehensive IVOC emission inventory for mobile sources in China, Sci. Total Environ., 851, 158312, https://doi.org/10.1016/j.scitotenv.2022.158312, 2022.

Zheng, H., Chang, X., Wang, S., Li, S., Yin, D., Zhao, B., Huang, G., Huang, L., Jiang, Y., Dong, Z., He, Y., Huang, C., and Xing, J.: Trends of Full-Volatility Organic Emissions in China from 2005 to 2019 and Their Organic Aerosol Formation Potentials, Environ. Sci. Technol. Lett., 10, 137-144, https://doi.org/10.1021/acs.estlett.2c00944, 2023.

Zhu, W., Zhou, M., Cheng, Z., Yan, N., Huang, C., Qiao, L., Wang, H., Liu, Y., Lou, S., and Guo, S.: Seasonal variation of aerosol compositions in Shanghai, China: Insights from particle aerosol mass spectrometer observations, Sci. Total Environ., 771, 144948, https://doi.org/10.1016/j.scitotenv.2021.144948, 2021.